Pergamon

Journal of Structural Geology, Vol. 16, No. 12, pp. 1641 to 1654, 1994

0191-8141/94 $7.00+0.00

0191-8141(94)E0013-O

Brittle deformation and fracture patterns on oceanic rift shoulders: the Esja peninsula, SW Iceland

THIERRY VILLEMIN

Laboratoire de Géodynamique, U.R.A. 69 C.N.R.S., Université de Savoie, BP 1104, 73011 Chambery Cedex, France

FRANÇOISE BERGERAT, JACQUES ANGELIER

Laboratoire de Tectonique quantitative, U.R.A. 1759 C.N.R.S., Université P. & M. Curie, 4, place Jussieu, 75252 Paris Cedex 05, France

and

CHRISTIAN LACASSE

The University of Rhode Island, Graduate School of Oceanography, Narragansett Bay Campus, Narragansett, RI 02882-1197, U.S.A.

(*Received* 3 *November* 1992; *accepted in revised form* 25 *January* 1994)

Abstract—This paper provides detailed structural data on the crustal deformation of the Esja peninsula, at the southwestern margin of the rift zone in SW Iceland. Forty percent of the faults are strike-slip with steep dips, 35% are normal dip-slip with dips ranging from 50° to 90°. For normal faults, E–W, NE–SW and NNE–SSW are the three major trends. The paleostress tensors determined using the fault data, indicate three main states of stress. Two extensional regimes (σ_3 N180°E ±10° and N110°E ±10°) are related to normal slip faults. The third is a compressive stress regime with σ_1 trending N10°E–N30°E. Associations between strike-slip and dip-slip faults are often observed, resulting from both the geometrical requirements of interactions between faulted blocks and from local–regional permutations between σ_1 and σ_2. We note a constant obliquity of 10–20° between the trend perpendicular to the regional structures and the computed direction of extension. This conclusion is also supported by the major trends of dykes and tensional fractures. There are two mechanisms of volcanic injection (local sheets and regional dykes) resulting in power-law cumulative thickness distributions with exponents of 1.5 and 3.0, respectively.

INTRODUCTION

In Iceland, more than 400 km of the axial rift zone of the Mid-Atlantic Ridge emerges (Fig. 1). On both sides of the active rift zone, there are inactive shoulders, mainly composed of basaltic rocks (Saemundsson 1979). This uplifted lava pile is deeply eroded and well exposed in cliffs along valleys and coasts (Fig. 2).

The Esja peninsula is at the southwestern margin of an emerged rift (Fig. 1). The exposed lava pile is more than 1000 m thick. This area is bounded by two large fjord-valleys formed by glacial erosion (Hvalfjordur and Kollafjordur-Mosfell, Fig. 2). The lava pile includes several small mountains (Eyrarfjall, Medalfell, Renivellir) and a large one (Esja), all containing well-exposed cliff sections. We made mainly qualitative observations in these cliffs, whereas most of our quantitative tectonic data were collected along the coastline and in several roadcuts and quarries.

Data on fault and slip orientations, as well as attitudes of dykes and tension fractures, were collected at several sites (Fig. 2). Normal faults and dykes are common at these sites. The host rock consists mainly of basaltic lava flows. The age of the lava pile generally decreases from the Plio-Pleistocene in the southeastern part of the study area, to the Pliocene in the northwestern part (Fig. 2).

THE REGIONAL FRACTURE PATTERN

Lineaments

The study of aerial photographs at the scale of 1:15,000 and 1:30,000 indicates a well-developed pattern of lineaments (Fig. 3b). From a regional point of view, the most common and most continuous lineaments strike NE–SW. Some can be traced over distances in excess of 2 km. As a first approximation, their spacing can be considered constant and averages 1 km. Two other sets of lineament trends can be identified. Their strikes are NW–SE (perpendicular to the first set) and NNE–SSW. These two sets are shorter than the first one and less developed.

Regional faults

About 50% of the NE–SW lineaments correspond to faults which could be identified in the field. Dykes are

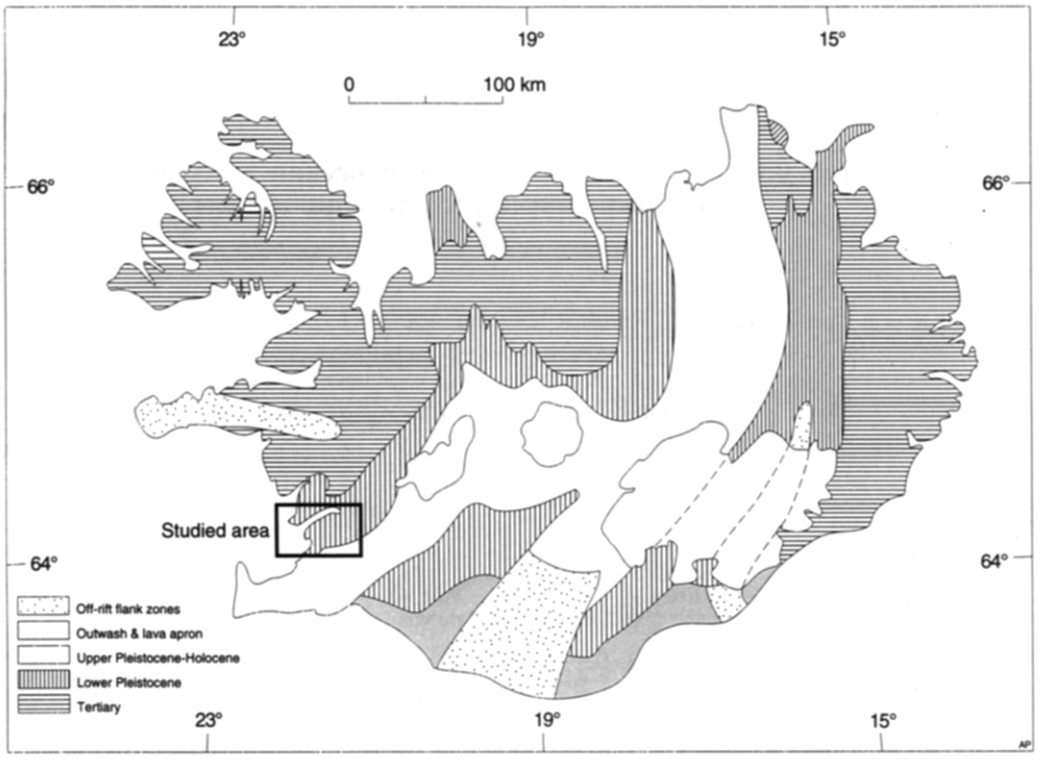

Fig. 1. Structural outline map of iceland (simplified after Saemundsson, 1986).

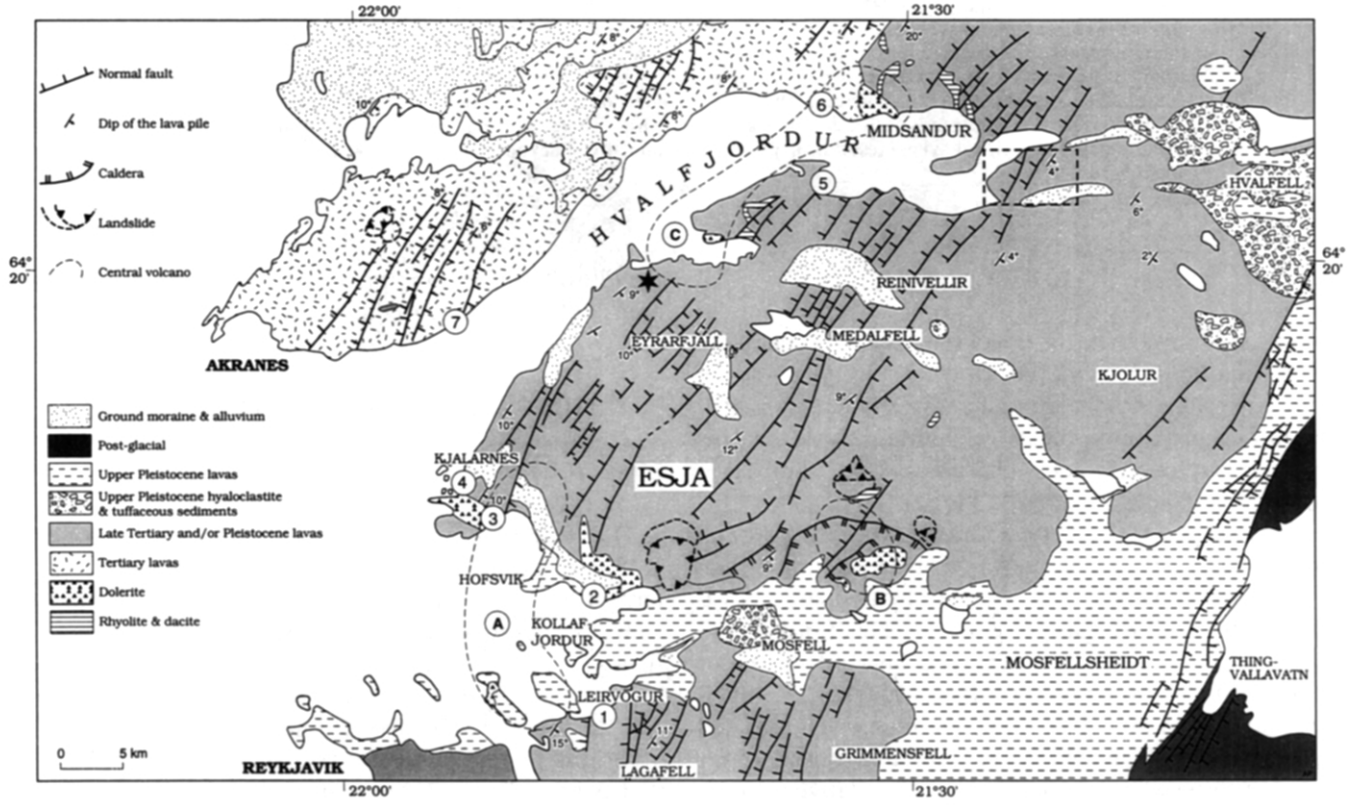

Fig. 2. Geological map of the study area (after Saemundsson & Einarsson 1980). Sites of data collection shown as circled numbers which are referred to in Figs. 5, 7 and 12. (1) Leirvogur; (2) Kollafjordur; (3) Hofsvik; (4) Kjalarnes, west coast; (5) Hvalfjordur, south coast; (6) Hvalfjordur, north coast; (7) Akranes, south coast. (A) Kjalarnes-Thverfell central volcano; (B) Stardalur central volcano; (C) Midsandur central volcano. Dashed rectangle, location of the horizontal view of Fig. 3(a); Star area displayed on the vertical view of Fig. 3(b).

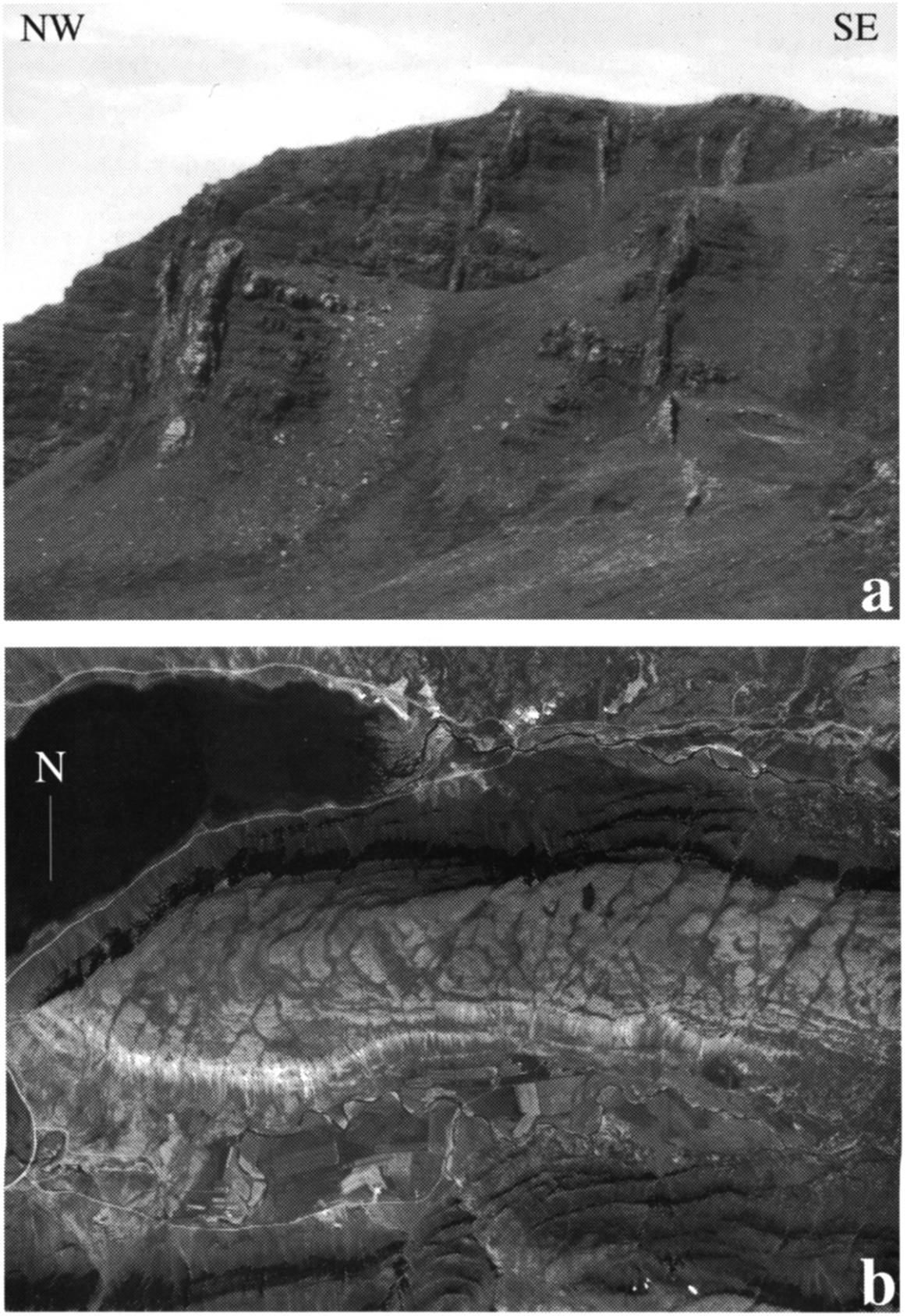

Fig. 3. The regional fracture pattern. (a) Dyke swarm on a horizontal view; (b) lineaments displayed on aerial photographs. See Fig. 2 for locations.

generally conspicuous on the aerial photographs and most of the shorter lineaments correspond to them. The views of the cliffs made in the field by photographic means (Fig. 3a) were compared with the vertical views of the same cliffs on the aerial photographs. Many lineaments identified on the top of the lava pile (on aerial photographs) are not related to any particular fractures observed in the corresponding vertical cross-sections. Such lineaments, apparently, correspond to joints which affect only the upper part of the lava pile.

Detailed field studies of the regional fractures have been made by Fridleifsson (1973) in the Esja area and Forslund & Gudmundsson (1991, 1992) in the northern part of the study area (the Akranes peninsula and eastern part of the Hvalfjordur area). The results can be compared with those from the southern and eastern areas adjacent to the study area (Gudmundsson 1986b, 1987b,c). All these results indicate that the NE–SW trending faults correspond to conjugate normal faults. Field evidence (Forslund & Gudmundsson 1991) indicates that a second family of normal faults with NNE–SSW trends also developed.

The normal faults affected the whole lava pile, resulting in block tilting. Fault displacements do not vary significantly from the bottom to the top of the lava pile (Gudmundsson 1984, Forslund & Gudmundsson 1991). These faults developed principally outside the active rift zone where lavas were continuously accumulating.

Note (1) that all faults show vertical displacements that commonly reach several meters (Forslund & Gudmundsson 1991, 1992), and (2) that the strike-slip component on these faults is difficult to estimate due to lack of geological markers. Both dip-slip and strike-slip slickenside lineations were observed on fault planes. A small strike-slip component on these regional faults is not incompatible with their being dominantly dip-slip.

Dykes swarms and cone sheets

Dykes are less regular in shape and attitude than faults. They generally belong to swarms (Gudmundsson 1983; 1984, Gautneb *et al.* 1989). Most dykes never reach the surface and they probably become longer and thinner with increasing depth (Gudmundsson 1990). Two different types of dyke swarms can be distinguished. The first type occurs near central volcanoes where the dykes are connected with a shallow crustal magma chamber around which they form a swarm of inclined sheets. The second type consists of regional dykes that have a great extent along strike.

Five large basaltic intrusions occur in the study area (Fig. 2) and are associated with three central volcanoes, namely, Kjalarnes-Thverfell, Hvalfjordur and Stardalur central volcanoes (Fig. 2). These volcanoes were active 2.8, 2.0 and 1.7 Ma ago respectively (Saemundsson & Einarsson 1980). These large intrusive bodies (more than 100 m thick) are mainly made of doleritic rocks. They are associated with dense swarms of basaltic cone sheets (e.g. the Kjalarnes-Thverfell central volcano), with collapse calderas (e.g. the Stardalur central volcano) or with rhyolitic domes and sheets (e.g. the Hvalfjordur central volcano).

The regional dykes are not confined to any particular central volcano. They have steep dips and are thick (more than 1 m). The steepest dipping dykes strike NE–SW (Forslund & Gudmundsson 1991, 1992). Dykes are presumed to have been emplaced by dilatation in a direction perpendicular to their trends. Matching pairs of angular contacts are common in thin dykes, although not in larger ones. In this former case, the determination of the dilatation direction (Bussell 1989) allows determination of the relative amplitude of shear component. However, the reconstructed shear component of the dyke opening is always small.

Structural setting and amount of extension

The structural pattern of the area considered corresponds to faulted blocks with an average width of 1 km, most of them being tilted to the east. However, E-dipping faults are as frequent as W-dipping ones (Forslund & Gudmundsson 1991). This implies that offsets are larger for W-dipping faults than for E-dipping ones. Crustal dilatation due to both regional dykes and faults averages 2% (Forslund & Gudmundsson 1991, 1992). The dilatation distribution is not homogeneous: crustal segments with high dilatation (>4%) alternate with segments with lower dilatation (<1%). This phenomenon seems to have a wavelength of roughly 2 km, as shown by detailed profiles from Forslund & Gudmundsson (1991).

MESOSCOPIC FAULTS AND THE MAIN STRESS FIELD

Fault types and orientations

Where outcrop conditions permit, analyses of fault data sets were carried out both in terms of fault-slip geometries and mechanisms and related paleostresses. Most faults observed are minor faults, with offsets smaller than 1 m.

Although the number and locations of our sites cannot be considered statistically representative for a regional distribution of faults orientations, some major characteristics are easily derived from the rose diagrams (Fig. 4). Some 340 faults with slickenside lineations were observed at six major sites (Fig. 2). These faults are mainly normal dip-slip and strike-slip, which represent 43% and 50%, respectively of our complete data set (Figs. 4d & e).

Figure 4(a) illustrates the distribution of fault types in our entire fault slip data set through a simple analysis of the relationships between dips of faults and pitches of striations. This diagram shows that several faults are strike-slip, with steep dips and shallow pitches (40% of data). Among this major subset, right-lateral and left-lateral faults are almost equal in number (Fig. 4a). Most remaining faults are normal dip-slip (35% of data), with

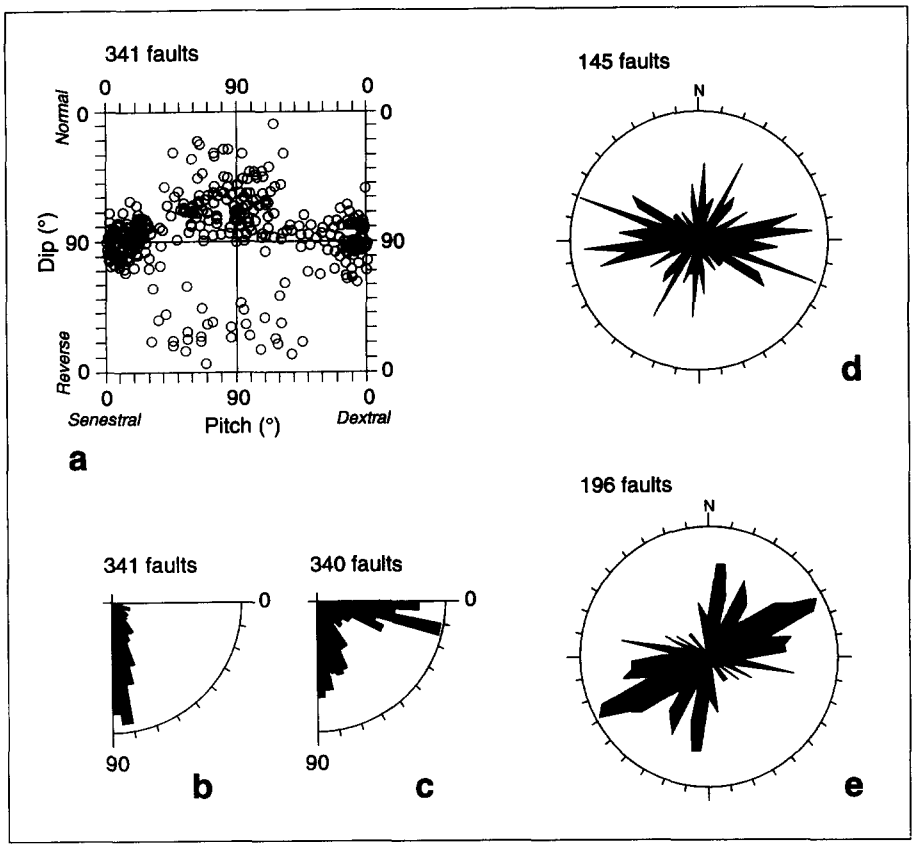

Fig. 4. Fault types and orientations. (a) Fault pitch vs fault dip; (b) rose diagram of fault dips; (c) rose diagram of pitches of slickenside lineations; (d) rose diagram of normal-slip fault strikes (145 measurements); (e) rose diagram of strike-slip fault strikes (196 measurements).

dips ranging from 50° to 90°. The remaining 25% are mainly oblique-slip faults with a few reverse faults.

The rose diagram of fault dips (Fig. 4b) shows that for 89% of the whole data set dips range from 50° (typical dip-slip faults) to 90° (typical strike-slip faults). In detail, however, there are numerous dip-slip faults that dip close to vertical (23% between 80° and 90°), and many strike-slip faults that dip between 50° and 70° (8%, Fig. 4a). Such apparent exceptions have two main origins. First, the tilting of large blocks has affected pre-existing faults, resulting in minor but significant changes in their dips. Faults strike approximately parallel to shallower dips for normal faults, and in deviations from vertical for strike-slip faults. Because stratum dips average 10° in the study area (Fig. 2), this effect plays a minor role. Second, detailed analyses of striations on fault surfaces revealed that in many cases both normal dip-slip and strike-slip movements occurred on the same fault surface. Depending on the original mechanism of the fault, such reactivations may result in various dip-pitch relationships, as discussed above (Fig. 4a), because the initial striations have often been erased. Similarly, many dip-slip normal faults were inherited from vertical structures such as joints, veins and dykes. Such reactivations explain the abnormally large proportion of very steep dips for the dip-slip fault subset and consequently for the whole data set (Figs. 4a & b).

The rose diagram of the pitches of slickenside lineations on fault planes (Fig. 4c) illustrates the difference between dip-slip and strike-slip fault mechanisms. Oblique-slip movements play a minor role although they are present in the data set (only 18% of pitches lie in the range between 30 and 60°). Note that the dispersion of pitches may be greater for early-stage faults, because of block tilting of about 10°.

The distribution of fault strikes is shown in two rose diagrams (Figs. 4d & e), in order to separate normal and strike-slip faults. For normal faults, there are three major trends, E–W, NE–SW and NNE–SSW (Fig. 4a). Our data set however cannot be considered representative at the regional scale, for two reasons. First, most of our sites are located along the fjords, which trend oblique to the major structural features of the area (Fig. 2). As a consequence, higher percentages of oblique trending fractures could be expected because Icelandic fjords commonly correspond to fracture zones. This particular location of our sites (Fig. 2) probably explains the high proportion of E–W normal fault strikes in our data set (Fig. 4), in comparison to the dominating NE–SW strike of the regional normal faults (Fig. 2). Second, all but few of the faults that we measured were minor, so that the difference between the two fault systems with contrasting maximum offsets may not be accounted for by our data. We suspect that such a scale cut-off contributes to magnify the apparent importance of E–W strikes in our data set (Fig. 4d), because at the scale of the

geological map of Fig. 2 all normal faults strike NE–SW, suggesting that E–W trending faults have limited lengths and offsets.

The diagram of strike-slip fault strikes shows several subsets (Fig. 4e). The significance of these subsets is discussed in the next subsection, based on mechanical analyses of individual sites (Fig. 5). As pointed out before (Bergerat *et al.* 1988, 1990), minor strike-slip faulting is very common and must be considered in paleostress reconstructions in Iceland. Except in particular areas such as transform fault zones, the strike-slip faults are generally very small despite their abundance. Thus, the relative importance of a subset within a set of minor fault slip data does not necessarily reflect the contribution of the corresponding fault slip geometry to the regional strain. Such a limitation was already mentioned for normal faulting (E–W vs NE–SW trends, Fig. 4d). This must be kept in mind, especially for strike-slip faults, where no offset distribution could be reliably identified due to the scarcity of suitable markers.

Paleostress regimes

The method that we used for reconstructing the paleostress at the sites shown in Fig. 2 consists of finding the best fit between observed directions and the sense of slip on faults and the theoretical shear stress induced on these planes by a common stress tensor. The inverse problem of computing this tensor from homogeneous sets of fault slip data was solved in our case by applying the direct inversion technique described by Angelier (1990). Because most sites revealed polyphase deformation, two or more paleostress tensors were computed, based either on preliminary selection of fault geometries (e.g. normal vs strike-slip) or on the dynamical separation of fault mechanisms and related tensors (Angelier 1984, 1989). Although the brittle deformation was clearly polyphase, our field data do not allow reliable reconstruction of the regional tectonic chronology. Data about relative chronology of fault movements were collected at various sites, but the corresponding succession of paleostresses differs from one place to another.

Figure 5 and Table 1 summarize the results of these paleostress determinations. The fault-slip data analysed are shown in the stereograms of Fig. 5. For each fault slip data subset, the attitudes of the calculated paleostress axes are given, as well as the ratio Φ between the principal stress differences (Table 1). These values correspond to the four variables of the reduced stress tensor (e.g. Angelier 1989, 1990). The principal stresses are referred to as σ_1 (maximum compressive stress), σ_2 (intermediate stress) and σ_3 (minimum stress).

$$\Phi = (\sigma_2 - \sigma_3)/(\sigma_1 - \sigma_3).$$

N–S extension related to normal slip on ENE–WSW to ESE–WNW trending faults is present in all sites but one (Fig. 5). WNW–ESE extension related to normal slip on N–S to NNE–SSW faults also occurs, in good agreement with the regional trend of extension which is N115°E on average (Gudmundsson *et al.* 1992, Bergerat *et al.* 1990). At the regional scale, the most significant extension has a WNW–ESE trend.

The paleostress patterns indicated by analyses of strike-slip fault data sets (and some reverse faults) are more complex (Fig. 5). However, two major patterns are identifiable in spite of uncertainties. For about one-half of paleostress fields, the extension trends approximately perpendicular to the major fault system of Fig. 2, while the σ_1 axes trend parallel to this system. This paleostress regime is thus characterized by the same WNW–ESE trend of σ_3 as that obtained from the extensional paleostress regimes discussed above, the main difference being the permutation between the σ_1 and σ_2 axes. This phenomenon of regional stress permutation has already been described and discussed in Iceland by Bergerat *et al.* (1990). For most other stress fields (Fig. 5), the direction of σ_1 axes ranges from being approximately perpendicular to being oblique at a large angle to the major fault trends of Fig. 2, hence oblique to the rift axis.

DYKES AND SHEETS

Dyke and sheet orientation distributions

More than 400 dykes and sheets have been observed in the southwestern part of the Esja peninsula (Fig. 6). Most of these dykes are near or within the doleritic intrusions of Kjalarnes and Tverfell (Fig. 2). Sheets are often rather irregular in shape and sometimes use preexisting fracture as channels; abrupt changes in strikes and dips are common. However, at the scale of the studied area, the orentation distribution of the sheets is rather regular (Fig. 6). Strikes and dips are variable, but for the entire data set, more than 80% of dykes strike in the azimuthal range 170°–220° (NNE–SSW on average).

Two characteristic sets of dykes dominate: (1) a set of NNE trending subvertical dykes apparently controlled by the regional stress field; and (2) a set of sheets with shallow dips and variable strikes was controlled by a local stress field.

The remaining dykes have trends in all directions, with dips varying from shallow to steep. Most of these dykes were controlled by local stress fields induced by their own magmatic pressure.

Note that the mean symmetry axis of the shallow-dipping sheets is not quite vertical but steeply dipping to the WNW; by contrast, the steeply dipping dykes shows a dominating dip to the ESE (Fig. 6). Thus, the complete set of dykes shown in Fig. 6 is apparently tilted by about 10° westwards. After backtilting by 10° towards the ESE, the mean symmetry axis of the first dyke set becomes vertical while that of the second set becomes horizontal. This geometry suggests that the whole dyke/sheet swarm was emplaced in a pile of horizontal lava flows and subsequently tilted about 10°.

The structural heterogeneity of the whole dyke/sheet set results from the interaction of WNW–ESE stretch-

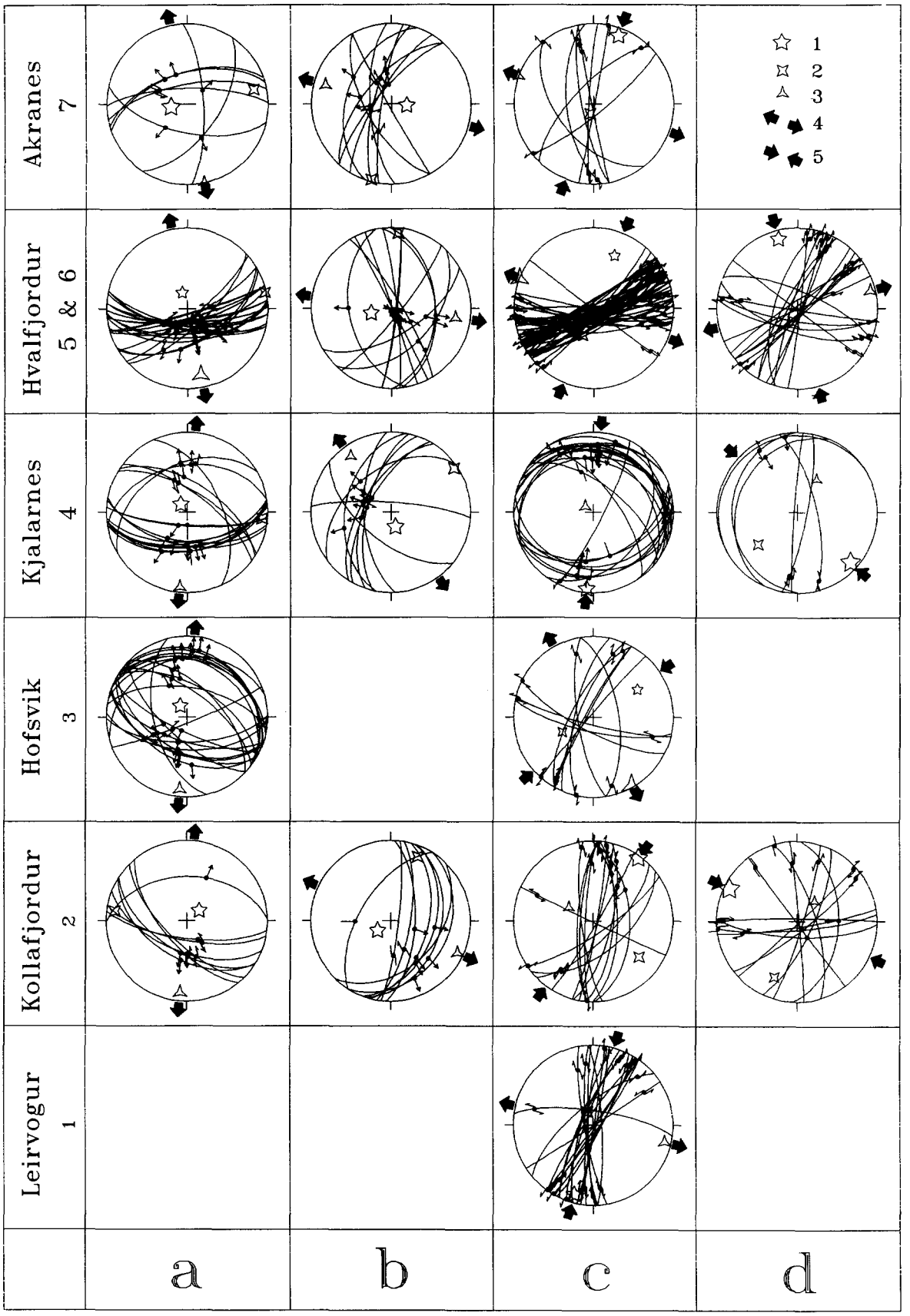

Fig. 5. Fault slip analysis and paleostress directions (Schmidt's projection, lower hemisphere). 1–7: numbers referring to the site locations shown in Fig. 2; (a) N–S extension; (b) WNW–ESE extension; (c) NNE–SSW compression; (d) NW–SE compression. Numerical values for the stress tensors are given in Table 1. σ_1, σ_2 and σ_3 are, respectively, given by (1), (2) and (3). Heavy arrows indicate directions of extension (4) or compression (5).

Table 1. Paleostress determinations from fault slip data: *P*: the tectonic stress regime *a–d*; see also Fig. 5. *N*: number of faults. σ_1, σ_2 σ_3: attitudes of the computed principal stress axes ($\sigma_1 > \sigma_2 > \sigma_3$, with compressions positive), with trend and plunge in degrees. Φ, ratio of principal stress differences, $\Phi = (\sigma_2 - \sigma_3)/(\sigma_1 - \sigma_3)$. *R*, ratio *v* defined by Angelier (1990) as a quality estimator of the inversion method for computing the stress tensor (in %, ranging from 0 to 200%). α, average angle between actual striae and computed shear, used as additional quality estimator (ranging from 0° to 180°). *Q*, overall quality estimator for the whole determination, taking into account quantitative, as well as the qualitative, parameters (quality decreases from *a*, excellent to *c*, poor)

Site	*P*	*N*	σ_1	σ_2	σ_3	Φ	*R*	α	*Q*
7-Akranes	*a*	7	261/73	78/17	168/1	0.3	34	11	*b*
	b	9	95/74	195/3	286/15	0.4	35	17	*c*
	c	8	20/11	200/79	290/0	0.3	42	11	*a*
	d	—	—	—	—	—	—	—	—
6-Hvalfjordur	*a*	21	343/73	78/2	169/17	0.8	27	13	*c*
	b	12	257/69	6/7	98/20	0.4	32	10	*b*
	c	43	22/30	201/60	292/0	0.9	36	15	*c*
	d	27	314/15	151/74	45/4	0.6	36	15	*a*
4-Kjalarnes	*a*	22	328/77	94/8	186/10	—	25	10	*a*
	b	—	—	—	—	—	—	—	—
	c	11	58/35	245/55	151/3	1	33	12	*a*
	d	—	—	—	—	—	—	—	—
S-Hofsvik	*a*	16	322/80	95/7	186/8	0.4	24	9	*a*
	b	8	174/72	49/10	316/14	0.4	24	8	*b*
	c	21	185/5	94/8	306/80	0.4	34	11	*a*
	d	8	133/10	231/37	30/51	0.2	30	8	*c*
2-Kollafjordur	*a*	8	51/74	278/11	185/11	0.5	14	6	*a*
	b	9	234/73	23/14	115/8	0.4	26	9	*a*
	c	15	36/3	128/28	299/62	0.3	28	14	*a*
	d	11	294/10	198/32	40/56	0	36	12	*b*
1-Leirvogur	*a*	—	—	—	—	—	—	—	—
	b	—	—	—	—	—	—	—	—
	c	21	195/11	336/75	104/9	0.4	49	13	*b*
	d	—	—	—	—	—	—	—	—

ing, which reflects the regional stress field (as shown by the consistent attitudes of the first set) with a local stress field related to magmatic overpressure in a shallow magma chamber.

Dyke/sheet thickness distributions

The cumulative distribution of dyke/sheet thicknesses in the Esja region is shown in Fig. 7 and compared with data from other areas of Iceland (Gudmundsson 1983, 1984, Gautneb *et al.* 1989, Forslund & Gudmundsson 1991) in Fig. 8. In these diagrams, the vertical *Y*-axis indicates the number $N(t)$ of dykes or sheets with thickness larger than t on the horizontal *X*-axis.

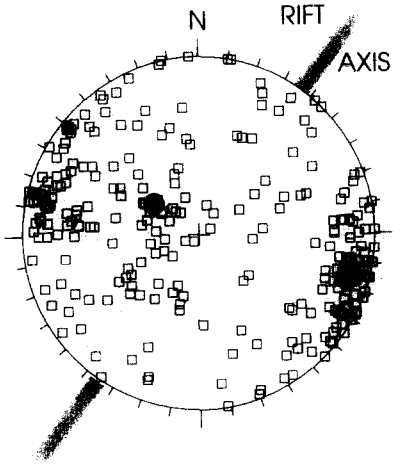

Fig. 6. Dykes and inclined sheets. Poles to all dykes measured in the study area are plotted as squares (Schmidt's projection, lower hemisphere). (a) Mean symmetry axis of the set of low-dip dykes; (b) mean symmetry axis of the set of high-dip dykes.

For each set plotted in Fig. 8, we must define a critical thickness T_c below which sampling is considered incomplete. Data on dyke thicknesses were collected along observation paths (such as the coast lines or road cuts). With such sampling, it is not possible to observe all thin dykes because they generally have small lengths and only part of them cross the observation paths. Using the data shown in Fig. 8 and taking this observation into account, we obtain the following statistical relationships (1) and (2), which can be considered satisfactory for thicknesses larger than T_c. We also tried to analyse the distribution of dykes thicknesses based on comparisons with statistical functions (e.g. Lognormal). We generally obtain poor correlation rates, except for the power laws (1) and (2) described below, which provide good fit with data:

$$(1) \quad N(t) = At^{-B} \quad \text{for } t < \tau$$

$$(2) \quad N(t) = A't^{-B'} \quad \text{for } t > \tau.$$

In these equations, τ is a particular thickness (5 m) which corresponds to a change in the slope of the linear curve, A and A' are parameters which increase with the total number of data and have a local significance, and B

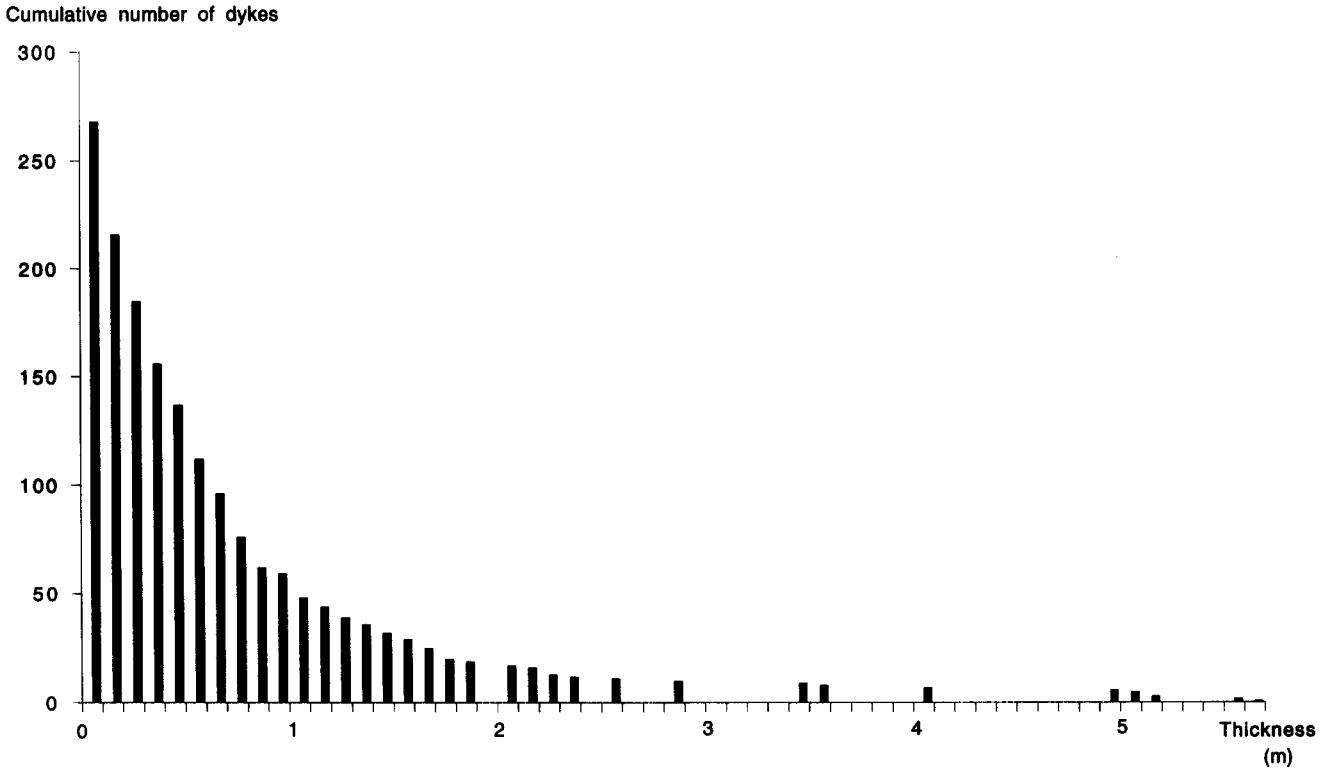

Fig. 7. Cumulative thickness distribution of dykes from the Esja peninsula.

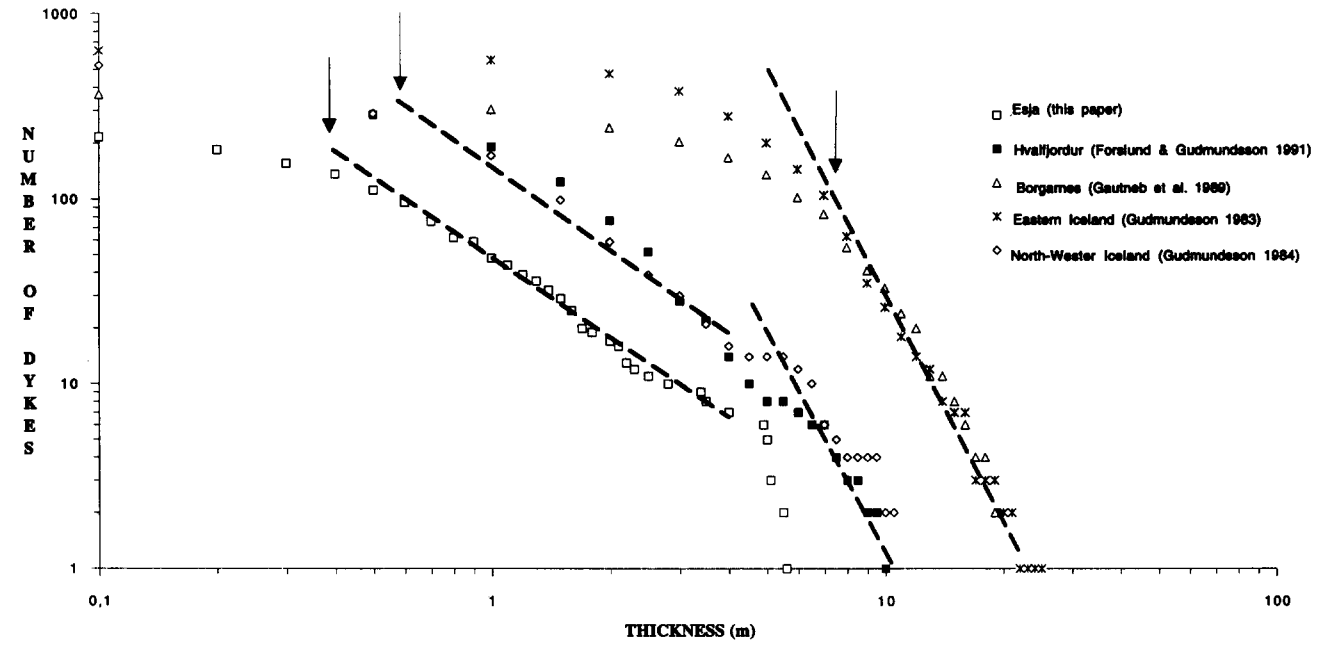

Fig. 8. Cumulative thickness distribution of dykes from Esja and other areas in Iceland.

and B' are constants with average values of 1.5 and 3.0, respectively. These two power laws correspond to two different mechanisms of dyke injection:

First mechanism. The first mechanism is associated with the formation of a local sheet swarm and corresponds to equation (1) where the exponent B equals 1.5. There the volcanic material is injected from a shallow magma chamber (Gudmundsson 1987a). Local stress fields due to the magmatic pressure in such chambers influence the geometry of dykes, leading to very variable strikes and dips of the sheets. The cumulative distribution decreases as a power law function with a power-law exponent of 1.5.

Second mechanism. The second mechanism is associated with the formation of a regional dyke swarm and corresponds to equation (2) where the exponent $B' = 3$. Subparallel regional dykes occur outside central volcanoes and are of greater volumes than the local sheets

(Gudmundsson 1987a). Presumably much of the corresponding volcanic material comes directly from reservoirs of partial melt at the bottom of the crust. Such a high value for exponent B' implies that most dyke thicknesses tend to be in a short range (5 m to several tens meters). The critical thickness Tc bounds the strong increase of number of dykes as dyke thickness decreases. The mechanical explanation for the empirical relationships remain unclear. Physical models of dykes injection (Gudmundsson 1983, 1986, 1988) do not allow determination of the distribution of dyke thicknesses with time, because these thicknesses depend on the evolution of magmatic overpressure for which no datum is available in our case.

Main trend of stretching

A three-dimensional estimate of stretching has been made by taking into account the orientation and thickness of each dyke. We assume that the opening of the dyke occurred almost perpendicular to the dyke plane. To obtain the stretching value in a given three-dimensional direction, we summed up all the thicknesses of dykes that trend perpendicular to this direction. Then the values were normalized by the maximum value and the contours drawn. We recognize that the role of host-rock elasticity during the process of increasing tensile stress and dyke opening may affect such estimates of stretching, but this effect is certainly minor.

The results are shown in Fig. 9. Five areas have thus been distinguished. We also computed the relative stretching rates for the complete data set (Fig. 7).

Assuming that opening occurs parallel to the minimum principal stress axis (σ_3), we can determine the orientation of σ_3 for the different subsets in Fig. 9. In all cases, σ_3 strikes N90°E to N120°E and is not quite horizontal but slightly tilted, probably due to block tilting.

Considering only the most steeply dipping dykes, we computed the cumulative and mean thicknesses of dykes for each orientation (Fig. 10). These diagrams show that the dykes striking between N0°E and N40°E correspond to the maximum cumulative and mean thicknesses. Outside this strike range the frequency and cumulative thicknesses of dykes markedly decrease.

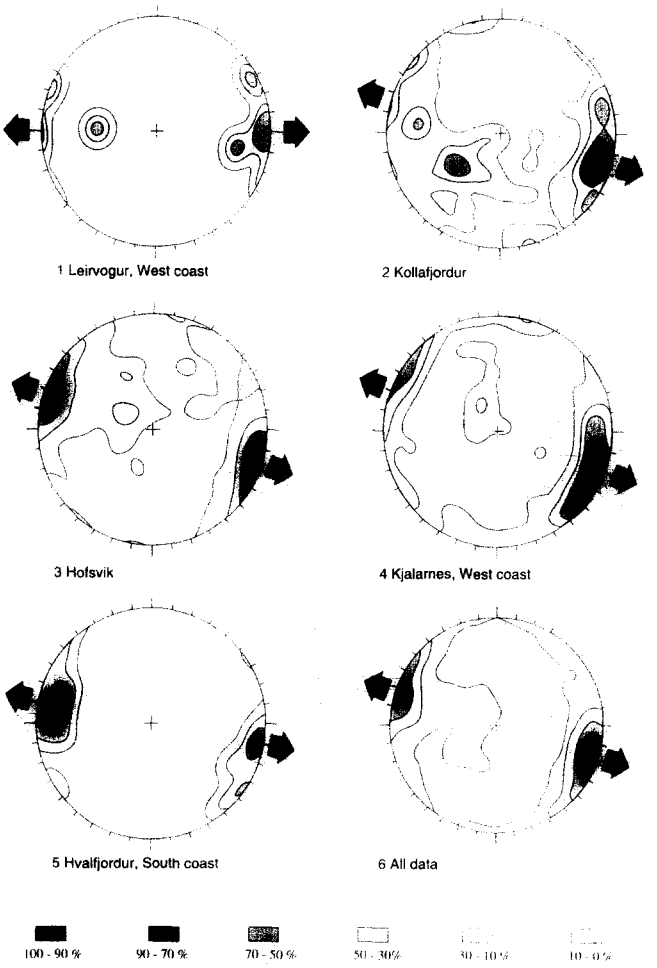

Fig. 9. Estimates of stretching orientations due to dykes and sheets. Contours of extension. All values are normalized by the maximum stretching value. Numbers refer to site locations shown in Fig. 2. (Schmidt's projection, lower hemisphere.)

FRACTURE GEOMETRY AND INFERRED STRESSES

In the study area we observed more than 500 mineral veins. These veins are filled with calcitic or phyllosilicic material. They are thin (from a few millimetres to a few centimetres) and their spacing is very variable. The length of the veins varies from 10 cm to several metres. They have steep dips (more than 70°, Fig. 11). Some mineral veins were emplaced in old columnar joints, which are overlaid by crystal fibres.

Four directional subsets were distinguished (Fig. 12). A N20°E trending subset is present everywhere and normally dominates. N80°E, N120°E and N170°E subsets are associated with this first subset.

From a geometrical point of view, the four subsets of mineral veins are mutually perpendicular. The dominant N20°E and N120°E subsets are perpendicular as well as the N80°E and N170°E subsets. These four subsets could correspond to perpendicular joint sets. If the joints originated as pure tension fractures (mode I fractures), they should be statistically perpendicular to the average σ_3 axis. Then one subset could be generated by the regional stress field and the perpendicular subset would result from inversion between the minimum (σ_3) and the intermediate (σ_2) axes. This inversion could have happened during stress relaxation following extension and normal faulting.

The two subsets thus distinguished can be related to two different states of stress. The N20°E and N120°E subsets correspond to the regional state of stress, that is, a WNW–ESE trending σ_3 stress. The N80°E and N170°E subsets may be related to the N–S extension, which we reconstructed independently by means of fault analysis (as pointed out in an earlier section).

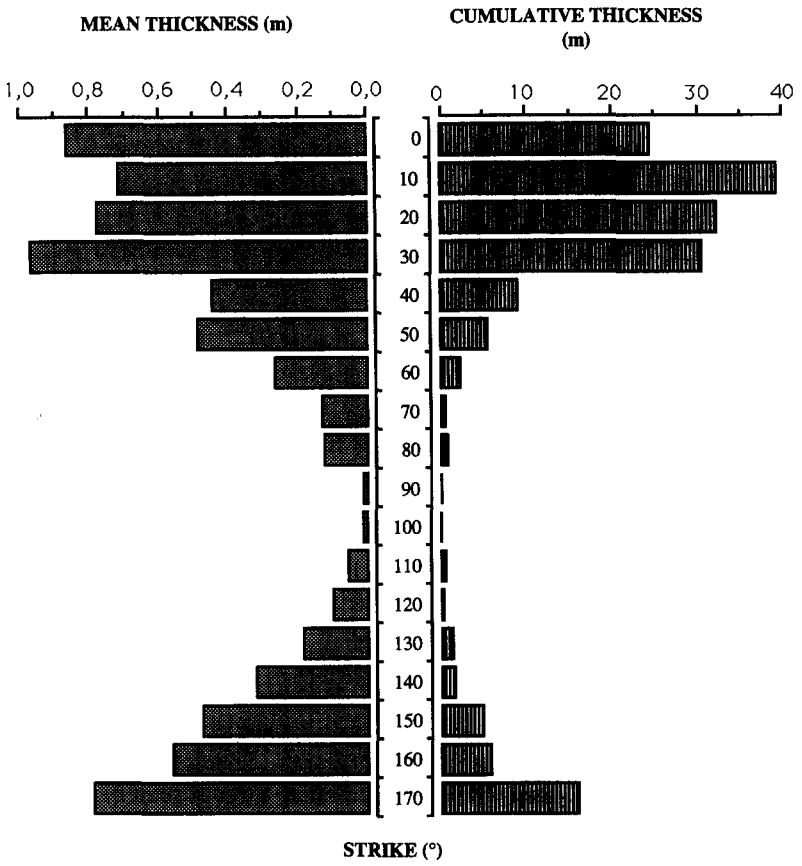

Fig. 10. Cumulative and mean thickness distributions as functions of trends for all dykes dipping more steeply than 60°.

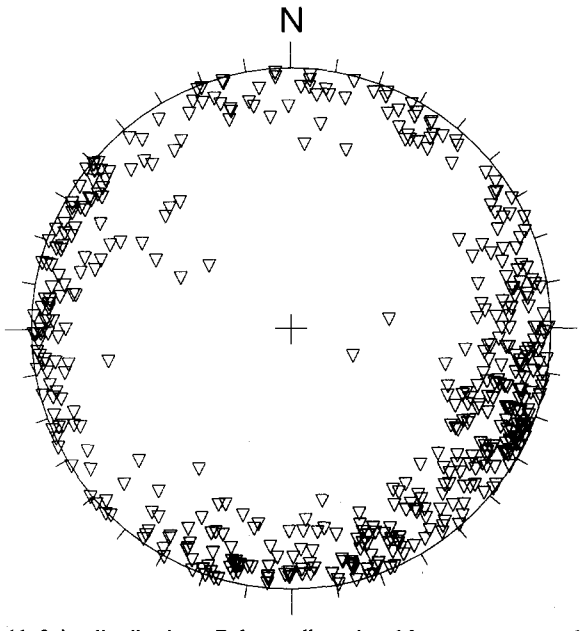

Fig. 11. Joint distributions. Poles to all tensional fractures measured in the studied area are plotted as triangles (Schmidt's projection, lower hemisphere).

DISCUSSION AND CONCLUSIONS

Significance of compression parallel to the rift zone

Numerous strike-slip movements have been found on micro-fault surfaces in the study area. Unlike dip-slip movements, where the maximum stress axis (σ_1) is vertical, these strike-slip displacements are related to a horizontal σ_1 axis. The existence of strike-slip faulting in Iceland outside transform fault zones, has been pointed out by Bergerat *et al.* (1989, 1990). There is a striking relationship between the paleostress axes based on dip-slip and strike-slip faults: the σ_3 axes are identical and the difference between the two regimes result only from a permutation between σ_1 and σ_2. The strike-slip faults, however, contribute little or very little to the total strain, because they are mesoscopic structures with small displacements.

This association between strike-slip and dip-slip movements is very common in extensional regimes (Angelier & Bergerat 1983, Bergerat 1987, Michel-Noel 1988, Bergerat *et al.* 1988). Bergerat *et al.* (1990) propose several hypotheses in order to explain this association. In Iceland, the association between dip-slip and strike-slip faults may result from both the geometrical need to conserve volume (in response to stretching) and the permutation of σ_1/σ_2 during normal faulting and dyke emplacement.

Significance of compression perpendicular to the rift zone

This paleostress regime is indicated not only by the relatively common occurrence of strike-slip faults (Bergerat *et al.* 1990), but also by several low angle reverse faults. This direction of compression is consistent with the results of *in situ* stress measurements by Haimson & Rummel (1982) in the Hvalfjordur area, indicating a

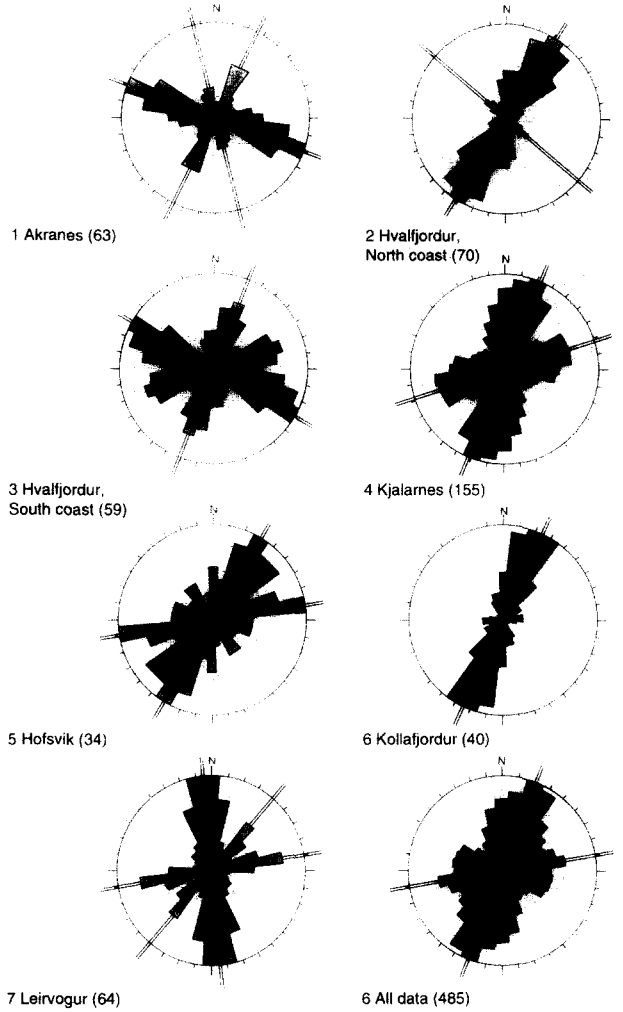

Fig. 12. Azimuth rose diagrams of the strikes of mineral veins. Numbers refer to site locations shown in Fig. 2.

NW–SE trending maximum horizontal stress. We interpret this compression perpendicular to the rift axis as related to the lateral loading of the crust accompanying dyke injection in the axial rift.

Evidence of N–S extension

The great importance of N–S extension in our results (Fig. 5) is mostly related to the particular situation of our data collection sites along, or close to, E–W fjords and corresponding fracture patterns.

The tectonic significance of these E–W fracture zones cannot be directly related to the actual spreading of the NE–SW trending rift zone. The Borgarfjördur earthquakes of 1974 (Einarsson *et al.* 1977) took place a few tens of kilometres north of the area studied and its focal mechanism indicates N–S tension. Note that the field evidence indicates that the fault slip related to this N–S extension occurred partly before and partly after the WNW–ESE stretching.

The N–S extension (or NNE–SSW) can be explained by loading within the rift zone (Gudmundsson *et al.* 1992). Then the rift zone is regarded as analogous to a mode I crack loaded by internal magmatic overpressure.

Partly, the N–S extension could be related to the N–S extension occurring in the Snaefells peninsula. Iceland is generally considered a hot spot (Wilson 1965, Morgan 1972) and the Snaefellsness zone has been interpreted as the failed arm of a triple junction (Burke & Dewey 1973, Sigurdsson 1970, Einarsson 1986).

General tilting and block rotation

The lava flows accumulate at the surface of the rift zone (Fig. 13) and tilt gently towards the active zone when they drift laterally and become part of the inactive shoulders of the rift (Walker 1959). On these shoulders, the estimated thickness of the lava pile is 5 km on average (Saemundsson 1979). Lava dip increases with depth and the lava groups become thicker down dip (Walker 1959). During crustal spreading, the lava pile gradually becomes dissected by normal faults which tilt the blocks towards the axis of the rift zone. In the area

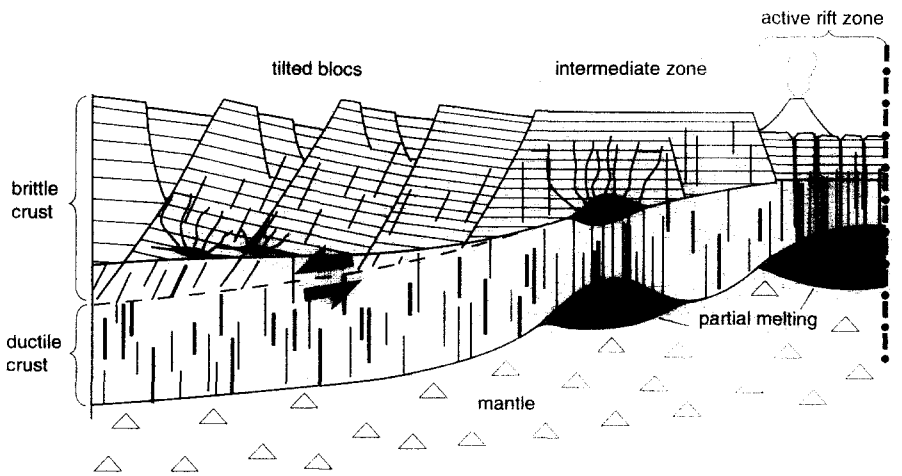

Fig. 13. Schematic section of a pattern of tilted blocks on the Icelandic rift shoulder. From right to left *Active rift zone*: lava accumulation, dyke emplacement, opening fracture and fault zone. *Intermediate zone*: the top of the lava pile recently accumulated is not affected by significant faults. Note that the lowest sections of the pile result from the outward shift of an oldest rift zone (as described above). *Tilted block zone*: due to cooling, the thickness of the brittle crust increases. The sense of shear controlled by gravity controls the vergence of normal faults.

studied, these blocks are bounded by normal faults dipping mostly to the west.

Two main hypotheses can explain the dip of these faults. The first model is based on the mechanical constraint pointed out by Gudmundsson (1992). Nucleation of faults may be controlled by the existence of preexisting en-échelon columnar joints that are perpendicular to lava flows. The second model assumes a mechanical control due to the underlying crustal deformation (Faugere & Brun 1984). In extensional areas the sense of tilt may be controlled by the sense of shear at the bottom of the brittle crust. In Iceland, the increasing thickness of the lava pile (mostly brittle) and its cooling during lateral transport imply that the limit between brittle and ductile crust dips away from the rift (Fig. 13). The sense of shear on this boundary should be controlled by gravity effects acting within the upper lithosphere.

Trend of the actual rift and direction of extension

Although the trends of the rift zone and the direction of extension are perpendicular in first approximation (Bergerat *et al.* 1990, Gudmundsson *et al.* 1992), the data presented in this study show an obliquity of 10°–20° between the trend perpendicular to that of regional structures and the computed directions of extension. As shown above, regional fractures are parallel to the actual rift and trend N35°E to N45°E. Assuming these fractures to be pure dip-slip faults or pure tension fractures, the direction of σ_3 should be N125°E to N135°E. The σ_3 axis, independently computed from analyses of minor fault-slip data as well as from the mean orientations of dykes and tensional fractures, trends in the azimuthal range N90°E–N110°E. This obliquity cannot be explained by a local effect of magmatic overpressure because it was observed throughout the whole area studied in a consistent way.

In Southwest Iceland, crustal spreading probably occurs in several steps (Gudmundsson *et al.* 1992). Taking this evolution into account, the observed obliquity described in the present paper may simply result from changes in the regional stress field through time (thus, small structures should have developed first). This interpretation implies, however, that no reactivation of these small structures occurred in a statistically significant way during the last step of the spreading process which is unlikely. For these reasons, and taking our observations into account, the hypothesis of major changes in stress field orientation should be abandoned. The second and most reasonable explanation implies that a slightly oblique rifting occurs in Southwest Iceland, with a small strike-slip component (10–20% of the total motion) on regional faults and regional dykes. This component should be left-lateral on all NE–SW trending normal faults, in order to accommodate the deformation with the N110°E mean σ_3 axis.

Acknowledgements—We thank A. Gudmundsson for information on the Esja area and helpful comments on the manuscript. The authors also thank A. Zanchi for constructive reviews and comments. We thank the French Embassy in Rekjavik for help. This work was supported by grants from the French–Icelandic scientific cooperation program (the Icelandic Ministry of Education and Culture and the French Ministère des Affaires étrangéres) and from the D.B.T.-I.N.S.U. French program (contribution number 658).

REFERENCES

Angelier, J. 1984. Tectonic analysis of fault slip data sets. *J. geophys. Res.* **89**, 5835–5848.

Angelier, J. 1989. From orientation to magnitudes in paleostress determinations using fault slip data. *J. Struct. Geol.* **11**, 37–50.

Angelier, J. 1990. Inversion of field data in fault tectonics to obtain the regional stress-III. A new rapid direct inversion method by analytical means. *Geophys. J.* **103**, 363–376.

Angelier, J. & Bergerat, F. 1983. Systèmes de contrainte et extension intracontinentale. *Bull. Cent. Rech. Explor. Prod. Elf-Aquitaine* **7**, 131–147.

Bergerat, F. 1987. Stress fields in the European Platform at the time of Africa–Eurasia collision. *Tectonics* **6**, 99–132.

Bergerat, F., Angelier, J. & Villemin, T. 1988. Systèmes de failles et états de contrainte sur une dorsale océanique émergée: l'Islande. *C. R. Acad. Sci., Paris* **307**, 1397–1403.

Bergerat, F., Angelier, J. & Villemin, T. 1990. Fault systems and stress patterns on emerged oceanic ridges: a case study in Iceland. *Tectonophysics* **179**, 183–197.

Burke, K. & Dewey, J. F. 1973. Plume-generated triple junctions: key indicators in applying plate tectonics to old rocks. *J. Geol.* **81**, 406–433.

Bussel, M. A. 1989. A simple method for the determination of the dilatation direction of intrusive sheets. *J. Struct. Geol.* **11**, 679–687.

Einarsson, P. 1986. Seismicity along the eastern margin of the North American plate. In: *The Geology Of The North America* (edited by Vogt, P. R. & Tucholke, B. E.). *Geol. Soc. Am.* **M**, 99–116.

Einarsson, P., Klein, F. W. & Bjornsson, S. 1977. The Borgarfjördur earthquakes of 1974 in West Iceland. *Bull. Seismol. Soc. Am.* **67**, 187–208.

Faugere, E. & Brun, J. P. 1984. Modélisation expérimentale de la distension continentale. *C. R. Acad. Sci., Paris* **299**, 365–370.

Fridleifsson, I. 1973. Petrology and structure of the Esja quaternary volcanic region, Southwest Iceland. Unpublished Ph.D., University of Oxford.

Forslund, T. & Gudmundsson, A. 1991. Crustal spreading due to dikes and faults in Southwest Iceland. *J. Struct. Geol.* **113**, 443–457.

Forslund, T. & Gudmundsson, A. 1992. Structure of Tertiary and Pleistocene normal faults in Iceland. *Tectonics* **11**, 57–68.

Gautneb, H., Gudmundsson, A. & Oskarsson, N. 1989. Structure, petrochemistry and evolution of a sheet swarm in an Icelandic central volcano. *Geol. Mag.* **126**, 659–673.

Gudmundsson, A. 1983a. Stress estimates from the length/width ratios of fractures. *J. Struct. Geol.* **5**, 623–626.

Gudmundsson, A. 1983b. Form and dimensions of dykes in eastern Iceland. *Tectonophysics* **95**, 295–307.

Gudmundsson, A. 1984. Tectonic aspects of dykes in North-western Iceland. *Jökull* **34**, 81–96.

Gudmundsson, A. 1986a. Formation of crustal magma chambers in Iceland. *Geology* **14**, 164–166.

Gudmundsson, A. 1986b. Mechanical aspects of postglacial volcanism and tectonics of the Reykjanes Peninsula, Southwest Iceland. *J. geophys. Res.* **91**, 12711–12721.

Gudmundsson, A. 1987a. Formation and mechanics of magma reservoirs in Iceland. *Geophys. J. Roy. astron. Soc.* **91**, 27–41.

Gudmundsson, A. 1987b. Geometry, formation and development of tectonic fractures on the Reykjanes Peninsula, Southwest Iceland. *Tectonophysics* **139**, 295–308.

Gudmundsson, A. 1987c. Tectonics of the Thingvellir fissure swarm, SW Iceland. *J. Struct. Geol.* **9**, 61–69.

Gudmundsson, A. 1990. Emplacement of dikes, sills and crustal magma chambers at divergent plate boundaries. *Tectonophysics* **176**, 257–275.

Gudmundsson, A. 1992. Formation and growth of normal faults at the divergent plate boundary in Iceland. *Terra Nova.* **4**, 464–471.

Gudmundsson, A., Bergerat, F., Angelier, J. & Villemin, T. 1992. Extensional tectonics of Southwest Iceland. *Bull. Soc. géol. Fr.* **163**, 561–570.

Haimson, B. C. & Rummel, F. 1982. Hydrofracturing stress measurements in the Iceland research drilling project drill hole at Reydarfjordur, Iceland. *J. geophys. Res.* **87**, 6632–6649.

Michel-Noel, G. 1988. Mécanismes et évolution de l'extension intra-

continentale des "Basin and Range", et développement tectonique des bassins sédimentaires. *Mém. Sci. Terre Univ. Curie, Paris* **88–42**, 215.

Morgan, W. J. 1972. Plate motions and deep mantle convection. *Mem. Geol. Soc. Am.* **132**, 7–22.

Saemundsson, K. 1979. Outline of the geology of Iceland. *Jökull* **29**, 7–28.

Saemundsson, K. 1986. Subaerial volcanism in the western North Atlantic. In: *The Geology of the North America* (edited by Vogt, P. R. & Tucholke, B. E.). *Geol. Soc. Am.* **M**, 69–85.

Saemundsson, K. & Einarsson, S. 1980. Geological map of Iceland, sheet 3, SW-Iceland. Museum of Natural History and the Iceland Geodetic Survey, Reykjavik, Iceland.

Sigurdsson, H. 1970. Structural origin and plate tectonics of the Snaefellsnes volcanic zone, Western Iceland. *Earth Planet. Sci. Lett.* **10**, 129.

Turcotte, D. L. & Oxburgh, E. R. 1973. Mid-Plate tectonics. *Nature* **244**, 337–339.

Walker, G. P. L. 1959. Geology of the Reydarfjordur area, eastern Iceland. *Quart. J. Geol. Soc. Lond.* **114**, 367–397.

Wilson, J. T. 1965. Evidence from ocean islands suggesting movement in the Earth. *Phil. Trans. Roy. Soc. Lond.* **258**, 145–167.